Augmentation of Universal Potentials for Broad Applications

Joe Pitfield,* Florian Brix, Zeyuan Tang, Andreas Møller Slavensky, Nikolaj Rønne, Mads-Peter Verner Christiansen, and Bjørk Hammer†

Center for Interstellar Catalysis, Department of Physics and Astronomy, Aarhus University, DK-8000 Aarhus C, Denmark

(Received 19 July 2024; accepted 2 January 2025; published 4 February 2025)

Universal potentials open the door for DFT level calculations at a fraction of their cost. We find that for application to systems outside the scope of its training data, pretrained CHGNet [Deng *et al.*, Nat. Mach. Intell. **5**, 1031 (2023)] has the potential to succeed out of the box, but can also fail significantly in predicting the ground state configuration. We demonstrate that via fine-tuning or a Δ-learning approach it is possible to augment the overall performance of universal potentials for specific cluster and surface systems. We utilize this to investigate and explain experimentally observed defects in the Ag(111)-O surface reconstruction and explain the mechanics behind their formation.

DOI: 10.1103/PhysRevLett.134.056201

Atomic structure plays a crucial role in the understanding and development of new materials and technologies. A great many different compounds have structures which have been determined by experimental observation through a variety of techniques [1–5]. However, the configuration space of potential structures increases exponentially with degrees of freedom as we combine surfaces with adsorbates, defects, alloys, and interfaces. Theoretical structure prediction offers the opportunity to screen and predict the structural properties of such systems. Studies of surface structure [6,7], catalysis [8–11], and interface physics [12–15] provide valuable insight into not only the interesting material properties of these systems, but also the key limitations of first principles methods in addressing these ever more configurationally complex problems.

Machine learning models offer the ability to reduce the amount of expensive first principles calculations performed, and the possibility of extending the results of small calculations to larger systems without the corresponding cubic [16] increase in cost common to density functional theory. Machine learning has been applied in a variety of ways to alleviate the computational workload of materials science: neural network potentials [17–23] and Gaussian process regression [24–30] for energetic evaluation, reinforcement [31–33], and active learning [15,34] for candidate structure suggestion. Such methods reduce the demand for expensive first principles calculations, provided sufficient training data. However, during the initialization of such approaches, acquiring sufficient data often remains expensive. Recent interest has surrounded the utilization of comprehensive structural databases such as the Materials Project [35], the OpenCatalyst Project [36] and PubChem [37] in training potentials which are broadly applicable. These so-called *universal potentials* theoretically remove the expensive initialization step of any materials science workflow, promising orders of magnitude decrease in cost for calculations of DFT level accuracy. Recent examples include M3GNet [38], MACE [39], AisNet [40], CHGNet [41], and DPA2 [42]. This Letter will focus on CHGNet, as it suggests strong performance with relatively few parameters (∼450 000).

CHGNet is trained on the Materials Project dataset [43], which is dominated by structures that fall into the bulk regime. Unsurprisingly, CHGNet has been demonstrated to perform well when applied to materials in this realm [41]. However, the majority of device physics occurs in regimes where the materials deviate from perfect bulk crystals: interfaces have drastically varying conductivities [13,44–49], defects play a key role in electronics [50–52], surfaces are defining in heterogeneous catalysis [53–55], and nanoparticulate phases are key in atmospheric [56] and astrochemical [57–59] contexts.

In this Letter, we investigate with CHGNet the structural properties of two sets of materials involving either nanoparticles or ultrathin oxides on a surface. Varying the system size and stoichiometry, we find for both types of materials that the universal potential is sufficiently accurate to identify the global minimum (GM) energy structures of some of the systems studied. However, we also find cases in which CHGNet lacks such accuracy. These cases form the basis for testing how to improve the pretrained CHGNet (v0.3.0). We pursue two avenues for this. Either we fine-tune the network, or we add an extra machine learning model to the potential prediction in what is known as Δ-learning [60].

The letter is organized in the following manner: First we present two silicate clusters, and augment the CHGNet energy predictions where necessary, following either a

*Contact author: joepitfield@gmail.com
†Contact author: hammer@phys.au.dk

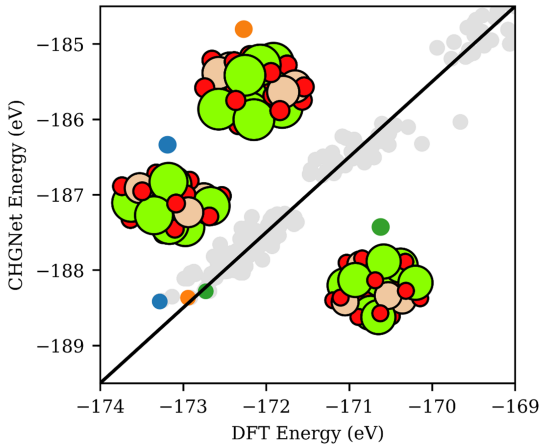

FIG. 1. Parity plot of CHGNet prediction vs DFT energy for four formula unit olivine clusters. Three unique low-energy configurations are illustrated and corresponding datapoints indicated. The solid line is a guide to the eye. Green, tan, and red spheres represent magnesium, silicon, and oxygen atoms, respectively.

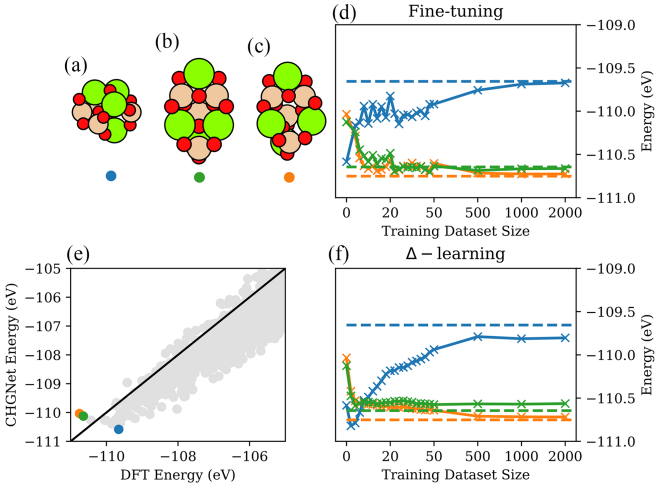

FIG. 2. (a)–(c) Three low energy cluster configurations of PYR-4. (e) Parity plot of the CHGNet vs DFT energies. (d) Fine-tuning prediction of energies with increasing data. (f) Δ-model prediction of energies with increasing data. Structures (a)–(c) are color coded in all cases, with dashed lines indicating DFT energies.

fine-tuning or Δ-learning strategy. Next, the effect of the augmentations is discussed as a function of the amount of data used. The letter proceeds to consider CHGNet predictions for ultrathin oxides on the Ag(111) surface. Augmentation is found necessary for experimental consistency, and the Δ-correction scheme is employed leading to the construction of a reliable model. Finally, the model is applied to very large surface defect structures containing more than 1000 atoms.

Throughout this Letter, we will utilize optimization methods as implemented in the "Atomistic Global Optimization X" package, AGOX(v3.6.0) [61] that builds on the "Atomic Simulation Environment" (ASE) [62]. Density functional theory (DFT) calculations are performed in GPAW [63]. More details on the methods used are given in Sec. S II, which also provides comparison to VASP, and Sec. S IV of Supplemental Material [64].

Beginning with the examination of silicate clusters, Fig. 1 presents three low energy configurations found for a silicate nanoparticle with four olivine formula units, i.e., $[Mg_2SiO_4]_4$. For these configurations, we find that CHGNet correctly predicts the same ordering as DFT [72]. This is evidenced by the parity plot of CHGNet versus DFT energies presented. We find similar DFT reproducibility behavior of CHGNet for a range of other structures, see Sec. S I [64]. This result demonstrates that despite CHGNet being trained largely on extended solid materials, it contains sufficient chemical insight so as to deal with the chemical consequences of compounds having finite size whereby many atoms end up in surface sites.

The offset of CHGNet energy to DFT energies apparent from Fig. 1 stems from the use of different DFT codes and DFT settings. The CHGNet architecture comes with 94 parameters, one for each atomic species, known as the *composition model*, which may be altered to accommodate such energy differences. Section S V of [64] discusses how to adjust the composition model parameters and eliminate the offset.

Using CHGNet (or other universal potentials, see discussion of Fig. S 8 [64]) for a wide variety of materials, we find occasional examples where it does not provide the same minimum energy configuration as found with DFT. An example of this is given in Figs. 2(a)–2(c), which presents three low-energy configurations of silicate nanoparticles with four pyroxene formula units, i.e., $[MgSiO_3]_4$ (PYR-4). In this case, the CHGNet model predicts the wrong stability ordering of the cluster configurations, as seen from the parity plot in Fig. 2(e). The structure preferred in CHGNet, Fig. 2(a), is hollow, while the one preferred in DFT [65], Fig. 2(c), is more compact.

To rationalize CHGNet's behavior for this system, we note that it relies on extrapolating the total energy of unknown systems by generalizing from local atomic descriptors in known systems. These descriptors result from graph embedding in consecutive deep neural network layers, and predictions for certain motifs may be off, if these are not present in the training data. We observe a consequence of this error while calculating the total dipole moments of the CHGNet and DFT minima, which yields 1.22 and $< 0.01|e| \cdot$ Å, respectively. The much higher value of the CHGNet minimum occurs with the presence of magnesium coordinated magnesium in a triangular motif capped by a single oxygen, cf. upper part of structure in Fig. 2(a). We theorize that this motif has been incorrectly extrapolated from structures in which it correlates with stability.

Postulating thusly, the obvious solution is to augment the model with a collection of appropriate data. In the following we shall take two approaches to such augmentation.

We first consider the option of fine-tuning CHGNet [73,74]. Fine-tuning involves (i) Acquire N_{sub} pieces of data, that specify structures and corresponding DFT energies and forces. (ii) Split the data in training and validation data randomly in some desired ratio, e.g., 90:10. (iii) Complete a training step in which the network parameters are updated via back propagation of the training data. (iv) Repeat steps until the model prediction accuracy on the validation set cannot be improved any further.

Figure 2(d) shows the energy prediction for the three low-energy cluster configurations of PYR-4 as a function of the amount of data, $1 \leq N_{\text{sub}} \leq 2000$, randomly extracted from an established dataset. Details of this dataset are given in the Sec. S V I [64]. As successively more data is used, the fine-tuned CHGNet learns the relative ordering of the three low-energy cluster configurations. For quantities of data points below 50 the fine-tuned CHGNet reacts turbulently to new data with predictions fluctuating in a unpredictable manner. When these fluctuations settle for $N_{\text{sub}} \geq 500$, the fine-tuned CHGNet matches well the DFT energies of the respective structures.

Having seen that it is possible for fine-tuned CHGNet to learn system specific information and attain ordering of structures on the PES that matches DFT, we now present an alternative approach: Δ-learning. The motivation for developing a new approach stems from the fact that, depending on the dataset size and the number of required training steps, the augmentation of a neural network via fine-tuning may be highly computationally costly, demanding expensive GPUs.

Δ-learning is an established machine learning approach in which one model learns "as much as it can" and a subsequent model learns the residual errors. Together, we refer to this combination of two models as a Δ-model. Δ-learning has previously been successfully applied in the domain of molecular [75] and materials [76] modeling, among others [60,77–83].

In the present context, we opt to use a Gaussian process regression (GPR) model for learning the residuals between the CHGNet and DFT values. We select GPR as an auxiliary model for its performance in the low data regime, both in terms of speed and reliability. Depending on hyperparameters, a GPR should further excel, preventing alteration to CHGNet predictions outside the regions of the data used for the GPR training. This is unlike the situation in which a neural network is used as the auxiliary model, where such alterations could be more far reaching in impact. See Sec. S VIII for an illustration of this behavior.

In the Δ-model approach we make predictions according to

$$E_{\Delta\text{-model}}(\mathcal{S}) = E^{\text{CHGNet}}(\mathcal{S}) + \sum_{i}^{N} \Delta E^{\text{GPR}}(\mathbf{x}_i), \quad (1)$$

for an unknown structure, $\mathcal{S}$, with local atomic representations $\mathbf{x}_i$. The GPR model energy prediction for the residual can be seen in Sec. S III [64]. We note that it is instructive to think of a Δ-model, composed of a fixed NN and a trainable GPR model, as a GPR model with a prior given by the NN, which is concurrent with the language within the AGOX implementation. The Δ-model approach does not require the expensive GPU retraining of the neural network as was the case with the fine-tuning approach. In practice, we use a local SOAP-descriptor-based sparse GPR model, see Sec. S III [64] for more details [66,67]. It would be equally viable to select any equivalently representative descriptor, including the intrinsic CHGNet features.

Figure 2(f) presents the prediction of the GPR-based Δ-model as a function of the amount, N_{sub}, of data subsampled from the dataset. The silicate cluster stabilities predicted with the GPR-based Δ-model are seen to smoothly tend towards the DFT values, i.e., they are not as inconsistent for $N_{\text{sub}} \leq 50$, and converge for $N_{\text{sub}} \geq 500$. The ordering becomes correct much earlier for the Δ-model, being consistently so after as little as 20 data points. This evidences that the GPR-based auxiliary model is sufficiently versatile to learn the residuals in the space defined by the silicate clusters considered.

At this point, it is instructive to discuss the origin of the dataset. The dataset was constructed in consecutive cycles of structural searches followed by model augmentation. Further details are given in Sec. S VI [64]. Here it suffices to highlight that such an active learning acquisition of training data is only computationally feasible if the model augmentation step is fast and stable with small additions of data. The differences in consistency between Figs. 2(d) and 2(f) in the low data regime, and the comparative training time (see Sec. S VIII [64]), confirms that datasets can be more efficiently incorporated with the GPR-based Δ model. This leads to Δ-models being overall powerful options when augmenting the predictive power of CHGNet or similar universal potentials.

We now move to consider an application involving surface reconstructions, where we will demonstrate the use of the Δ-model approach for system sizes not computationally accessible for DFT studies. Specifically, we shall consider three ultrathin oxide phases that have been observed on Ag(111) [84,85]. The phases are the $c(4 \times 8)$, $c(3 \times 5\sqrt{3})$, and $p(4 \times 5\sqrt{3})$, that have 0.5, 0.4, and 0.375 surface oxygen coverages, respectively. For convenience, we shall refer to the three phases as phase I, II, and III, respectively.

Starting with phase I, the insets in Fig. 3(a) present its structure and two alternative structures found when searching in either the CHGNet or in the full DFT energy

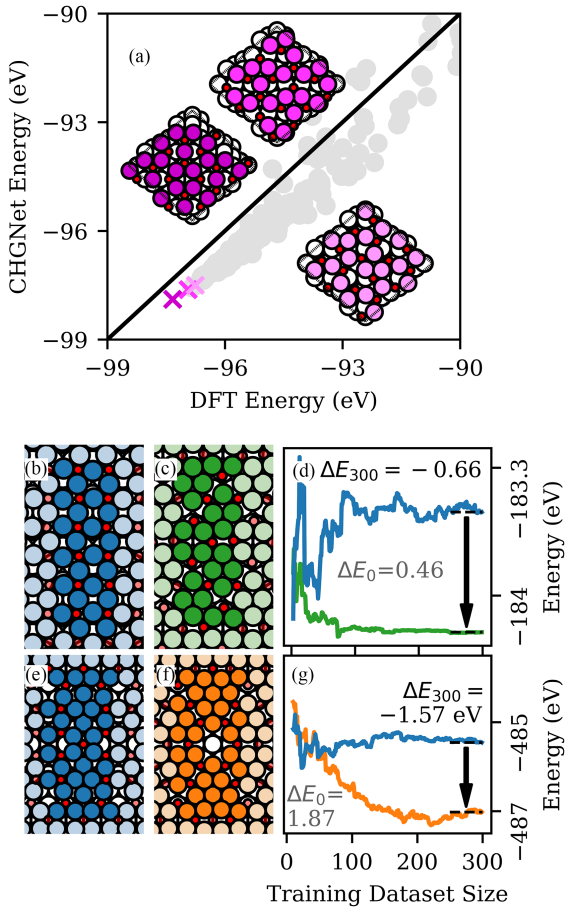

FIG. 3. (a) Parity plot of phase I structures, with color coded insets depicting their correspondingly colored points. DFT and CHGNet agree on the GM. (b) CHGNet GM for phase II. (c) DFT GM for phase II. (d) Δ-model prediction for phase II. The true energy difference when calculated with DFT is −0.53 eV. (e) CHGNet GM for phase III. (f) DFT GM for phase III. (g) Δ-model prediction for phase III. The true energy difference when calculated with DFT is −0.76 eV. In all depictions, red spheres represent oxygen, with all other colors indicating silver.

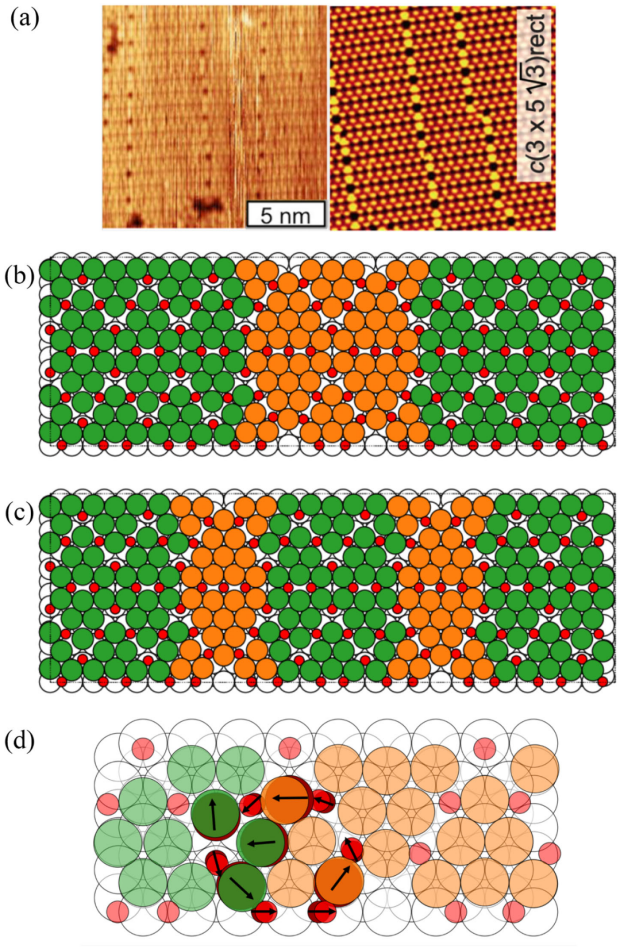

FIG. 4. (a) Reproduction of STM images: Reprinted with permission from Ref. [85]. Copyright 2016 American Chemical Society, and from Ref. [84] under the Creative Commons Attribution 3.0 License, respectively. Both images depict the phase II ultrathin oxide on Ag(111) under oxygen exposure, where single-width phase III stripes can be observed consistently. The structures shown depict (b) neighboring phase III cells, (c) dispersed III cells, and (d) the relaxation undergone at the interface between phases II and III.

landscape. The parity plot displayed in Fig. 3(a) shows that CHGNet works quite well for this system. Moving to phase II in Figs. 3(b) and 3(c), the situation changes and now CHGNet predicts a structure with linear O-Ag-O motifs lining up in rows as the more stable, Fig. 3(b), while DFT has an elaborate structure with Ag_6 triangles as the ground states, Fig. 3(c).

In order to remedy the deficient CHGNet prediction for the correct ground state structure for phase II, we collected training data via active learning, as outlined in Sec. S VII [64]. Figure 3(d) shows the prediction of the energy of structures with a Δ-model as a function of the amount of training data used. Here, we collected the data for the same cell as phase II itself, but for a range of stoichiometries, reducing the focus on the stoichiometry containing the solution. This demonstrates that the model is capable of learning the correct ordering and energy difference of the two structures.

Finally, in Figs. 3(e)–3(g) the situation for phase III is presented. Again, the pretrained CHGNet predicts the wrong ground state structure, Fig. 3(e), which does not have the Ag_6 and Ag_{10} triangular motifs that are present in the DFT ground state structure, Fig. 3(f). Now interestingly, the Δ-model that was trained for phase II, when applied to phase III is able to predict the correct ordering, and improve the energy difference, as shown in Fig. 3(g). This demonstrates that the Δ-model generalizes well and paves the way for its application to more advanced materials problems where DFT calculations become prohibitively large.

In Fig. 4 we present a case in which the Δ-model is applied to a large structure present in the Ag(111) surface

reconstruction. The STM images in Fig. 4(a), obtained independently by the groups of Refs. [84] and [85], suggest the appearance of single rows of the phase III structure inside larger domains of phase II. These defect rows are observed to move dynamically at room temperature and their presence therefore cannot be ascribed to kinetic limitations. To assess the possibility of a thermodynamic origin of the rows we adopted the Δ-model developed for Fig. 3. In Figs. 4(b) and 4(c) two systems are presented that explain why, for instance, the rows of phase III do not collapse to wider domains. In Fig. 4(b) two rows of phase III rows are adjacent to each other, and interfaced to phase II, while in Fig. 4(c) the two rows of phase III have dispersed into being fully separated by phase II. With the augmented CHGNet model, we can calculate the energy change of this process, and find it to be preferred by 0.352 eV, meaning that the interface energy between phase II and III is −0.176 eV per $5\sqrt{3}a/\sqrt{2}$ side length, where a is the lattice constant.

Figure 4(d) shows the considerable relaxations occurring at the interface between the two phases. Omitting the relaxations perpendicular to the interface plane the interface energy becomes essentially zero, leading us to the conjecture that stress present within phase II is relieved at the interface and constitutes the driving mechanism for the presence of the rows of phase III defects within the large domains of phase II. The reason why the system does not evolve into alternating single rows of either phase, which would maximize the amount of favorable interfaces, is that this would also bring down the overall oxygen coverage and hence chemisorption energy gain, given the difference in O-coverage of phase II and III.

In conclusion, we have investigated the capability of a universal potential, CHGNet, in describing selected inorganic clusters and surfaces. In cases where the accuracy of the pretrained CHGNet model is insufficient to correctly order low-energy structures, we demonstrate that either fine-tuning or Δ-learning offer a means to augment the model. We finally used a Δ-learning augmented CHGNet model to identify and rationalize negative energy domain boundaries in the thin film oxides forming on Ag(111).

Acknowledgments—We acknowledge support by VILLUM FONDEN through Investigator Grant, Project No. 16562, and by the Danish National Research Foundation through the Center of Excellence "InterCat" (Grant Agreement No. DNRF150).

[1] P. F. Fewster, Prog. Cryst. Growth Charact. Mater. **48**, 245 (2004).
[2] L. Stobinski, B. Lesiak, A. Malolepszy, M. Mazurkiewicz, B. Mierzwa, J. Zemek, P. Jiricek, and I. Bieloshapka, J. Electron Spectrosc. Relat. Phenom. **195**, 145 (2014).
[3] R. Černý, Crystals **7**, 142 (2017).
[4] A. Gloystein, N. Nilius, J. Goniakowski, and C. Noguera, J. Phys. Chem. C **124**, 26937 (2020).
[5] S. S. Shields and J. A. Gupta, Surf. Sci. **740**, 122403 (2024).
[6] G. Gutiérrez, A. Taga, and B. Johansson, Phys. Rev. B **65**, 012101 (2001).
[7] R. Zhang, L. Li, L. Frazer, K. B. Chang, K. R. Poeppelmeier, M. K. Chan, and J. R. Guest, Phys. Chem. Chem. Phys. **20**, 27456 (2018).
[8] B. L. Hendriksen, M. D. Ackermann, R. Van Rijn, D. Stoltz, I. Popa, O. Balmes, A. Resta, D. Wermeille, R. Felici, S. Ferrer *et al.*, Nat. Chem. **2**, 730 (2010).
[9] F. Polo-Garzon, Z. Bao, X. Zhang, W. Huang, and Z. Wu, ACS Catal. **9**, 5692 (2019).
[10] S. Chen, F. Xiong, and W. Huang, Surf. Sci. Rep. **74**, 100471 (2019).
[11] E. A. D. Baker, J. Pitfield, C. J. Price, and S. P. Hepplestone, J. Phys. Condens. Matter **34**, 375001 (2022).
[12] C. Hill, R. Beach, and T. McGill, J. Vac. Sci. Technol. B **18**, 2044 (2000).
[13] G. Schusteritsch, S. P. Hepplestone, and C. J. Pickard, Phys. Rev. B **92**, 054105 (2015).
[14] N. T. Taylor, F. H. Davies, I. E. M. Rudkin, C. J. Price, T. H. Chan, and S. P. Hepplestone, Comput. Phys. Commun. **257**, 107515 (2020).
[15] J. Pitfield, N. Taylor, and S. Hepplestone, Phys. Rev. Lett. **132**, 066201 (2024).
[16] S. Mohr, L. E. Ratcliff, L. Genovese, D. Caliste, P. Boulanger, S. Goedecker, and T. Deutsch, Phys. Chem. Chem. Phys. **17**, 31360 (2015).
[17] J. Behler and M. Parrinello, Phys. Rev. Lett. **98**, 146401 (2007).
[18] K. T. Schütt, H. E. Sauceda, P.-J. Kindermans, A. Tkatchenko, and K.-R. Müller, J. Chem. Phys. **148** (2018).
[19] O. T. Unke and M. Meuwly, J. Chem. Theory Comput. **15**, 3678 (2019).
[20] J. Gasteiger, F. Becker, and S. Günnemann, Adv. Neural Inf. Process. Syst. **34**, 6790 (2021).
[21] K. Schütt, O. Unke, and M. Gastegger, in *International Conference on Machine Learning* (PMLR, 2021), pp. 9377–9388.
[22] I. Batatia, D. P. Kovacs, G. Simm, C. Ortner, and G. Csányi, Adv. Neural Inf. Process. Syst. **35**, 11423 (2022).
[23] S. Batzner, A. Musaelian, L. Sun, M. Geiger, J. P. Mailoa, M. Kornbluth, N. Molinari, T. E. Smidt, and B. Kozinsky, Nat. Commun. **13**, 2453 (2022).
[24] A. Denzel and J. Kästner, J. Chem. Phys. **148** (2018).
[25] O.-P. Koistinen, V. Ásgeirsson, A. Vehtari, and H. Jónsson, J. Chem. Theory Comput. **16**, 499 (2019).
[26] O.-P. Koistinen, V. Ásgeirsson, A. Vehtari, and H. Jónsson, J. Chem. Theory Comput. **15**, 6738 (2019).
[27] V. L. Deringer, A. P. Bartók, N. Bernstein, D. M. Wilkins, M. Ceriotti, and G. Csányi, Chem. Rev. **121**, 10073 (2021).
[28] M. K. Bisbo and B. Hammer, Phys. Rev. B **105**, 245404 (2022).
[29] L. R. Merte, M. K. Bisbo, I. Sokolović, M. Setvín, B. Hagman, M. Shipilin, M. Schmid, U. Diebold, E. Lundgren, and B. Hammer, Angew. Chem. **134**, e202204244 (2022).
[30] Y. Hamamoto, T. N. Pham, M. K. Bisbo, B. Hammer, and Y. Morikawa, Phys. Rev. Mater. **7**, 124002 (2023).

[31] M. S. Jørgensen, H. L. Mortensen, S. A. Meldgaard, E. L. Kolsbjerg, T. L. Jacobsen, K. H. Sørensen, and B. Hammer, J. Chem. Phys. **151** (2019).

[32] Z. Zhou, S. Kearnes, L. Li, R. N. Zare, and P. Riley, Sci. Rep. **9**, 10752 (2019).

[33] T. Gogineni, Z. Xu, E. Punzalan, R. Jiang, J. Kammeraad, A. Tewari, and P. Zimmerman, Adv. Neural Inf. Process. Syst. **33**, 20142 (2020).

[34] J. S. Smith, B. Nebgen, N. Lubbers, O. Isayev, and A. E. Roitberg, J. Chem. Phys. **148**, 241733 (2018).

[35] K. A. Persson, B. Waldwick, P. Lazic, and G. Ceder, Phys. Rev. B **85**, 235438 (2012).

[36] L. Chanussot, A. Das, S. Goyal, T. Lavril, M. Shuaibi, M. Riviere, K. Tran, J. Heras-Domingo, C. Ho, W. Hu *et al.*, ACS Catal. **11**, 6059 (2021).

[37] S. Kim, P. A. Thiessen, E. E. Bolton, J. Chen, G. Fu, A. Gindulyte, L. Han, J. He, S. He, B. A. Shoemaker *et al.*, Nucl. Acids Res. **44**, D1202 (2016).

[38] C. Chen and S. P. Ong, Nat. Comput. Sci. **2**, 718 (2022).

[39] I. Batatia, P. Benner, Y. Chiang, A. M. Elena, D. P. Kovács, J. Riebesell, X. R. Advincula, M. Asta, W. J. Baldwin, N. Bernstein *et al.*, arXiv:2401.00096.

[40] Z. Hu, Y. Guo, Z. Liu, D. Shi, Y. Li, Y. Hu, M. Bu, K. Luo, J. He, C. Wang *et al.*, J. Chem. Inf. Model. **63**, 1756 (2023).

[41] B. Deng, P. Zhong, K. Jun, J. Riebesell, K. Han, C. J. Bartel, and G. Ceder, Nat. Mach. Intell. **5**, 1031 (2023).

[42] D. Zhang, X. Liu, X. Zhang, C. Zhang, C. Cai, H. Bi, Y. Du, X. Qin, J. Huang, B. Li *et al.*, arXiv:2312.15492.

[43] B. Deng, 10.6084/m9.figshare.23713842.v2 (2023).

[44] T. J. Marks, Angew. Chem., Int. Ed. Engl. **29**, 857 (1990).

[45] G. Chen, J. Heat Transfer **119**, 220 (1997).

[46] C.-W. Nan, G. Liu, Y. Lin, and M. Li, Appl. Phys. Lett. **85**, 3549 (2004).

[47] N. Burger, A. Laachachi, M. Ferriol, M. Lutz, V. Toniazzo, and D. Ruch, Prog. Polymer Sci. **61**, 1 (2016).

[48] S. Zhang, A. Hao, N. Nguyen, A. Oluwalowo, Z. Liu, Y. Dessureault, J. G. Park, and R. Liang, Carbon **144**, 628 (2019).

[49] Q. Liu, F. Wang, W. Shen, X. Qiu, Z. He, Q. Zhang, and Z. Xie, Ceram. Int. **45**, 23815 (2019).

[50] J. D. Bryan and D. R. Gamelin, Prog. Inorg. Chem. **54**, 47 (2005).

[51] B. I. Shklovskii and A. L. Efros, *Electronic Properties of Doped Semiconductors* (Springer Science & Business Media, New York, 2013), Vol. 45.

[52] C. Durand, X. Zhang, J. Fowlkes, S. Najmaei, J. Lou, and A.-P. Li, J. Vac. Sci. Technol. B **33**, 02B110 (2015).

[53] D. Rosenthal, Phys. Status Solidi (a) **208**, 1217 (2011).

[54] W. Huang and W.-X. Li, Phys. Chem. Chem. Phys. **21**, 523 (2019).

[55] F. Zaera, Coord. Chem. Rev. **448**, 214179 (2021).

[56] P. Biswas and C.-Y. Wu, J. Air Waste Manage. Assoc. **55**, 708 (2005).

[57] Z. Tang, F. D. S. Simonsen, R. Jaganathan, J. Palotás, J. Oomens, L. Hornekær, and B. Hammer, Astron. Astrophys. **663**, A150 (2022).

[58] A. P. Rasmussen, G. Wenzel, L. Hornekær, and L. H. Andersen, Astron. Astrophys. **674**, A103 (2023).

[59] V. Poterya, I. S. Vinklárek, A. Pysanenko, E. Pluharova, and M. Fárník, ACS Earth Space Chem. **8**, 369 (2024).

[60] R. Ramakrishnan, P. O. Dral, M. Rupp, and O. A. Von Lilienfeld, J. Chem. Theory Comput. **11**, 2087 (2015).

[61] M.-P. V. Christiansen, N. Rønne, and B. Hammer, J. Chem. Phys. **157** (2022).

[62] A. H. Larsen, J. J. Mortensen, J. Blomqvist, I. E. Castelli, R. Christensen, M. Dułak, J. Friis, M. N. Groves, B. Hammer, C. Hargus *et al.*, J. Phys. Condens. Matter **29**, 273002 (2017).

[63] J. J. Mortensen, A. H. Larsen, M. Kuisma, A. V. Ivanov, A. Taghizadeh, A. Peterson, A. Haldar, A. O. Dohn, C. Schäfer, E. Ö. Jónsson *et al.*, J. Chem. Phys. **160** (2024).

[64] See Supplemental Material at http://link.aps.org/supplemental/10.1103/PhysRevLett.134.056201 for further details and discussions (see also Refs. [63,65–71]). The topics covered include CHGNet out-of-the-box performance, DFT settings, local GPR, global optimization, composition model, silicate dataset creation, silver oxide dataset creation, comparison between fine-tuning and GPR and the robustness of the Delta model, and PYR-4 comparison with other universal potentials.

[65] A. M. Escatllar, T. Lazaukas, S. M. Woodley, and S. T. Bromley, ACS Earth Space Chem. **3**, 2390 (2019).

[66] A. P. Bartók, R. Kondor, and G. Csányi, Phys. Rev. B **87**, 184115 (2013).

[67] N. Rønne, M.-P. V. Christiansen, A. M. Slavensky, Z. Tang, F. Brix, M. E. Pedersen, M. K. Bisbo, and B. Hammer, J. Chem. Phys. **157**, 174115 (2022).

[68] J. P. Perdew, K. Burke, and M. Ernzerhof, Phys. Rev. Lett. **77**, 3865 (1996).

[69] A. H. Larsen *et al.*, J. Phys. Condens. Matter **29**, 273002 (2017).

[70] L. Himanen, M. O. J. Jäger, E. V. Morooka, F. Federici Canova, Y. S. Ranawat, D. Z. Gao, P. Rinke, and A. S. Foster, Comput. Phys. Commun. **247**, 106949 (2020).

[71] J. Laakso, L. Himanen, H. Homm, E. V. Morooka, M. O. Jäger, M. Todorović, and P. Rinke, J. Chem. Phys. **158**, 234802 (2023).

[72] A. M. Slavensky, M.-P. V. Christiansen, and B. Hammer, J. Chem. Phys. **159** (2023).

[73] B. Deng, Y. Choi, P. Zhong, J. Riebesell, S. Anand, Z. Li, K. Jun, K. A. Persson, and G. Ceder, arXiv:2405.07105.

[74] B. Focassio, L. P. M. Freitas, and G. R. Schleder, ACS Appl. Mater. Interfaces, (2024).

[75] S. Käser, O. T. Unke, and M. Meuwly, New J. Phys. **22**, 055002 (2020).

[76] A. Nandi, C. Qu, P. L. Houston, R. Conte, and J. M. Bowman, J. Chem. Phys. **154**, 051102 (2021).

[77] L. Hu, X. Wang, L. Wong, and G. Chen, J. Chem. Phys. **119**, 11501 (2003).

[78] R. M. Balabin and E. I. Lomakina, J. Chem. Phys. **131**, 074104 (2009).

[79] M. Gillan, D. Alfè, A. Bartók, and G. Csányi, J. Chem. Phys. **139**, 244504 (2013).

[80] P. Zaspel, B. Huang, H. Harbrecht, and O. A. von Lilienfeld, J. Chem. Theory Comput. **15**, 1546 (2018).

[81] S. Chmiela, H. E. Sauceda, K.-R. Müller, and A. Tkatchenko, Nat. Commun. **9**, 3887 (2018).

[82] H. E. Sauceda, S. Chmiela, I. Poltavsky, K.-R. Müller, and A. Tkatchenko, J. Chem. Phys. **150**, 114102 (2019).

[83] M. Stöhr, L. Medrano Sandonas, and A. Tkatchenko, J. Phys. Chem. Lett. **11**, 6835 (2020).

[84] J. Schnadt, J. Knudsen, X. L. Hu, A. Michaelides, R. T. Vang, K. Reuter, Z. Li, E. Lægsgaard, M. Scheffler, and F. Besenbacher, Phys. Rev. B **80**, 075424 (2009).

[85] J. Derouin, R. G. Farber, M. E. Turano, E. V. Iski, and D. R. Killelea, ACS Catal. **6**, 4640 (2016).